Thin Solid Films 520 (2012) 3593–3599

Contents lists available at SciVerse ScienceDirect

Thin Solid Films

journal homepage: www.elsevier.com/locate/tsf

Structural and morphological transformations of TiO_2 nanotube arrays induced by excimer laser treatment

Ming-Yi Hsu, Nguyen Van Thang, Chih Wang, Jihperng Leu *

Department of Materials Science and Engineering, National Chiao Tung University, 1001 University Road, Hsinchu 300, Taiwan, ROC

ARTICLE INFO

Article history:
Received 11 July 2011
Received in revised form 29 November 2011
Accepted 7 December 2011
Available online 16 December 2011

Keywords:
Anodic oxidation
Titanium dioxide
Nanotube arrays
Excimer laser annealing
Structural properties
X-ray diffraction
Scanning electron microscopy

ABSTRACT

The structural and morphological transformations of TiO_2 nanotube arrays (TNAs) treated by excimer laser annealing (ELA) were investigated as a function of the laser fluence using parallel and tilted modes. Results showed that the crystallinity of the ELA-treated TNAs reached only about 50% relative to that of TNAs treated by furnace anneal at 400 °C for 1 h. The phase transformation starts from the top surface of the TNAs with surface damage resulting from short penetration depth and limited one-dimensional heat transport from the surface to the bottom under extremely short pulse duration (25 ns) of the excimer laser. When a tilted mode was used, the crystallinity of TNAs treated by ELA at 85° was increased to 90% relative to that by the furnace anneal. This can be attributed to the increased area of the laser energy interaction zone and better heat conduction to both ends of the TNAs.

1. Introduction

In recent years, titanium dioxide (TiO_2) nanotube structures have stimulated significant interest due to their unique properties for use in various applications including electrochromic [1,2], photocatalytic devices [3], sensors [4], and solar cells [5–7]. Particularly in dye-sensitized solar cell application [5], it is well known that TiO_2 nanotube arrays (TNAs) constructed of oriented one-dimensional nanostructure, aligned perpendicular to the transparent conductive oxide substrate, can enhance electron transport and reduce recombination with redox electrolytes, leading to a higher charge collection efficiency [8]. Thus, various approaches such as template synthesis [9], hydrothermal reactions [10], and anodic oxidization [11] have been developed for preparing TiO_2 nanotube structure. Among these approaches, the anodic oxidization technique is the simplest and most straightforward approach to fabricate ordered TNAs. By controlling the electrochemical anodization parameters (applied potential, electrolyte compositions, electrolyte pH, temperature, etc.), one can obtain TNAs with various surface morphologies, tube diameters, lengths, and wall thickness [11,12].

In addition to the geometric shapes, the microstructure of TiO_2 is another critical property influencing TiO_2 applications. For example, for photocatalysis applications, the anatase phase is more active than the rutile phase due to its larger band gap and lower electron–hole recombination probability [8]. Also, increased degree of anatase phase in crystalline TiO_2 has been found to enhance the catalytic activity, for example, in the photocatalytic degradation of organic pollutants [13,14]. Such enhancement of photocatalytic activity could be attributed to the reduction of amorphous domains, defects, or impurities, which act as the recombination centers for photogenerated electrons and holes [15,16]. To increase the crystallinity of TiO_2 structure after formation, post annealing is typically required to change its structure from amorphous to anatase phase. Nevertheless, thermal annealing treatment using a conventional furnace anneal takes hours to complete the transformation of the crystal structure of the film. To expedite the annealing time or deliver low-temperature processing for flexible devices using polymer substrates with low glass transition temperature and poor thermal stability, excimer laser annealing (ELA) is one of the preferred fast processing technologies [17,18]. It has been reported that the phase transition from amorphous to anatase or rutile phase is observed within a nanosecond time scale by laser treatment [19,20]. So far, most studies have been carried out on TiO_2 powders [20] or thin films [21]. However, only a small depth of material is processed upon ELA irradiation because most extreme heating of pulsed laser annealing is confined to the near-surface region of the sample due to the short duration of the UV laser pulse. The challenge is to overcome the limited penetration depth in thick TNAs.

In this study, the evolution of morphology and microstructure in TNAs was investigated as functions of laser fluence. The mechanisms of phase transition and the changes of the surface of TNAs induced by laser are proposed. Furthermore, laser annealing in a tilted mode has been developed to resolve the limited penetration depth in a parallel

* Corresponding author. Tel.: +886 35131420; fax: +886 35724727.
E-mail address: jimleu@mail.nctu.edu.tw (J. Leu).

0040-6090/$ – see front matter © 2011 Elsevier B.V. All rights reserved.
doi:10.1016/j.tsf.2011.12.036

mode. Its difference in the structural and morphological transformation of TNAs will be examined and discussed.

2. Experimental details

2.1. Preparation of TNAs

Titanium foil (99.9% purity, 0.5 mm thickness) was used as the substrate for forming the TiO_2 layer by anodic oxidation. Prior to anodization, Ti foil was ultrasonically cleaned by distilled water, rinsed by acetone, and then dried by a purging N_2 gas. All anodization experiments were carried out at room temperature using a two-electrode electrochemical cell consisting of a stainless steel foil (SS304) as the cathode and a Ti foil as the anode, at a constant DC potential, 20 V for 24 h. In order to obtain TiO_2 nanotubes with high aspect ratio, we used a high-viscosity ethylene glycol electrolyte with 0.5 wt.% NH_4F and 3 wt.% H_2O. Fig. 1 illustrates the surface and cross-section morphology of TiO_2 nanotube arrays prepared by anodic oxidation in NH_4F solution. Surface morphology of the TiO_2 nanotube structure after treatment time of 24 h showed a tube diameter of 50 nm, wall thickness of 15 nm, and tube thickness of 7 μm (140:1 aspect ratio). The key for achieving such high-aspect-ratio growth is to adjust the ionic diffusion coefficient of the electrolyte, which is responsible for maintaining a high H^+ concentration at the pore bottom with a protective environment maintained along the pore walls and at the pore mouth during chemical drilling [11].

After fabrication, the samples were annealed by an excimer laser. Laser annealing was performed with a KrF excimer laser operated at 248 nm wavelength (Lambda Physik Complex 201), 25 ns pulse width and 10 Hz repetition rate. The diameter of the laser beam was adjusted to 0.5×1.5 cm^2 to ensure full coverage onto the TNA samples (sample size is 1×1.5 cm^2) by two separate exposures. The laser annealing conditions were selected to elucidate the structural and morphological transformation of TNAs by changing the laser fluence from 67, 125, 133, 267 to 400 mJ/cm^2 under the same number of 9000 shots. In this study, we also used two laser-sample irradiation modes for laser annealing of TNAs: (1) parallel mode and (2) tilted mode as schematically illustrated in Fig. 2a and b, respectively. In the parallel mode (Fig. 2a), the angle α between the laser beam and sample was set at 90° with a fixed substrate holder. In the tilted mode (Fig. 2b), the angle α (0°–90°) was varied from 30° to 85° in this study. In addition, the sample was rotated 40° manually around the axis of the laser beam for every 1000 shots to deliver a total of 9000 shots with uniformity. In order to compare any difference in the structure and morphology between laser annealing and conventional annealing, conventional annealing of TNA samples was carried out using a furnace in air atmosphere at 400 °C for 1 h [22].

2.2. Morphology and microstructure characterization of TNAs

The surface and cross-section morphology of TNAs were examined using a field emission scanning electron microscope (FESEM) (JOEL JSM-6700) operating at an accelerating voltage of 15.0 kV and focused ion beam scanning electron microscope (FIB/SEM) (FEI Nova-200) operating at an accelerating voltage of 5.0 kV. An X-ray diffractometer (XRD) (Siemens Diffractometer D5000) with Cu K_α ($\lambda = 1.5405$ Å) radiation at 40 kV and 30 mA in the Bragg-Bentano configuration was employed to analyze the crystal structure of the TNA films. In addition, transmission electron microscope (TEM) images and selected area diffraction (SAD) patterns of TNAs were obtained by a high-resolution transmission electron microscope (HRTEM) (JEOL 2010) at 200 kV.

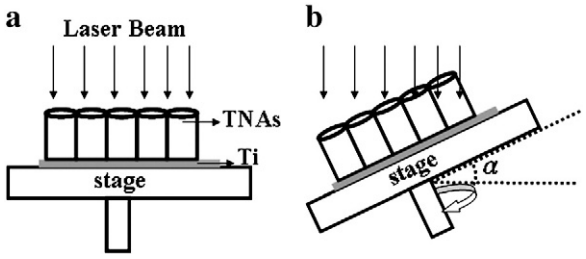

Fig. 2. Schematic diagrams of laser anneal systems for TNAs in (a) parallel mode and (b) tilted mode.

3. Results and discussions

3.1. ELA treatment of TNAs in a parallel mode

We first examined the laser fluence effect on TNAs prepared by anodic oxidation in parallel mode. Fig. 3 shows the XRD patterns of TNAs prepared by anodic oxidation as-grown in NH_4F solution and post annealing by excimer laser with various fluences at a total of 9000 shots. Results showed that the as-grown TNAs were fully amorphous because only the diffraction peaks from Ti substrate were detected. After irradiation of the TNAs with the excimer laser at 67 mJ/cm^2 laser fluence, the anatase phase appeared and the intensity of anatase (101) peak increased with increasing laser fluence up to 125 mJ/cm^2. As the fluence was further increased to ≥133 mJ/cm^2, the TNA film exhibited not only anatase (101) and (200) peaks, but also rutile (110), (101), and (111) peaks. The mechanism of the ELA TiO_2 crystallization process has been reported by Van Overschelde et al. [23]. The absorption of light occurs by exciting of the electrons from occupied to unoccupied energy states. This is because the photon energy, $h\nu$, is larger than the fundamental bandgaps of various TiO_2 phases (E_g are 3.0 eV for rutile, and 3.2 for anatase) [24]. The absorption of light creates an electron–hole pair by exciting an electron from the valence band into the conduction band. Since the optically excited states were obviously unstable, the system decays through a combination of various processes involving electrons, phonons, and atoms (or vacancies) which contribute to the heating of the lattices of the TiO_2 sample. When the heating is sufficient to overcome the

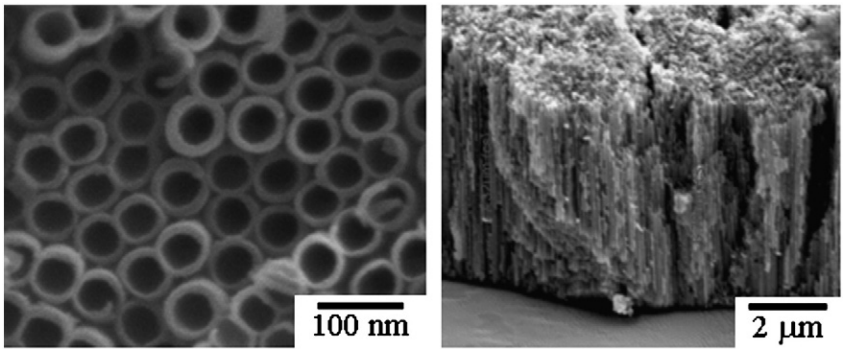

Fig. 1. Surface and cross-section morphologies of the TNAs prepared by anodic oxidation in NH_4F solution for 24 h.

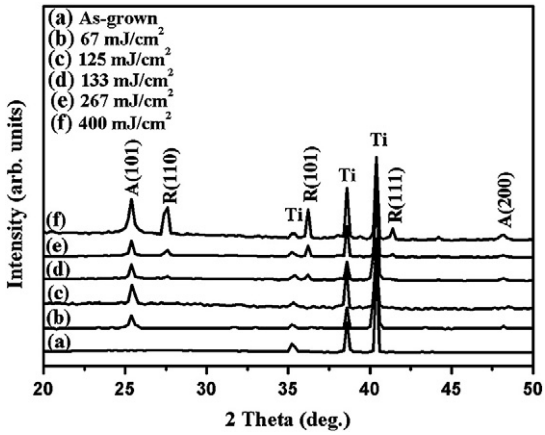

Fig. 3. XRD patterns of the TNAs prepared by anodic oxidation in NH_4F solution (as-grown) and annealing by excimer laser with various fluences at 9000 shots.

nucleation barrier, phase transitions may occur. Hence, in this case, the laser energy overcame the nucleation barrier for transformation of amorphous TiO_2 to anatase and possibly rutile phase. In addition, the amount of crystallinity of TNA films increased with increasing laser fluence.

The surface and cross-section morphology evolution of the TNAs annealed by excimer laser with various fluences were examined by SEM as shown in Fig. 4. A gradual change in surface morphology with increasing laser fluence was observed. For laser annealing under the laser fluence at 67 mJ/cm^2 (Fig. 4a), the surface morphology of highly ordered nanotube structure showed only slight damage, while the bulk of the nanotube arrays still remained intact. As the fluence was increased to 125 and 133 mJ/cm^2 (Fig. 4b and c), significant roughening and flower-like layers were observed on the top surface. As the fluence was further increased to 267 mJ/cm^2 (Fig. 4d), a re-solidified layer was formed on the surface, which sealed off some of the opening of the nanotubes. Finally, such morphology became more obvious for the samples treated at 400 mJ/cm^2 (Fig. 4e), while the bulk of the nanotube arrays remained intact. In short, the surface temperature of TiO_2 increased

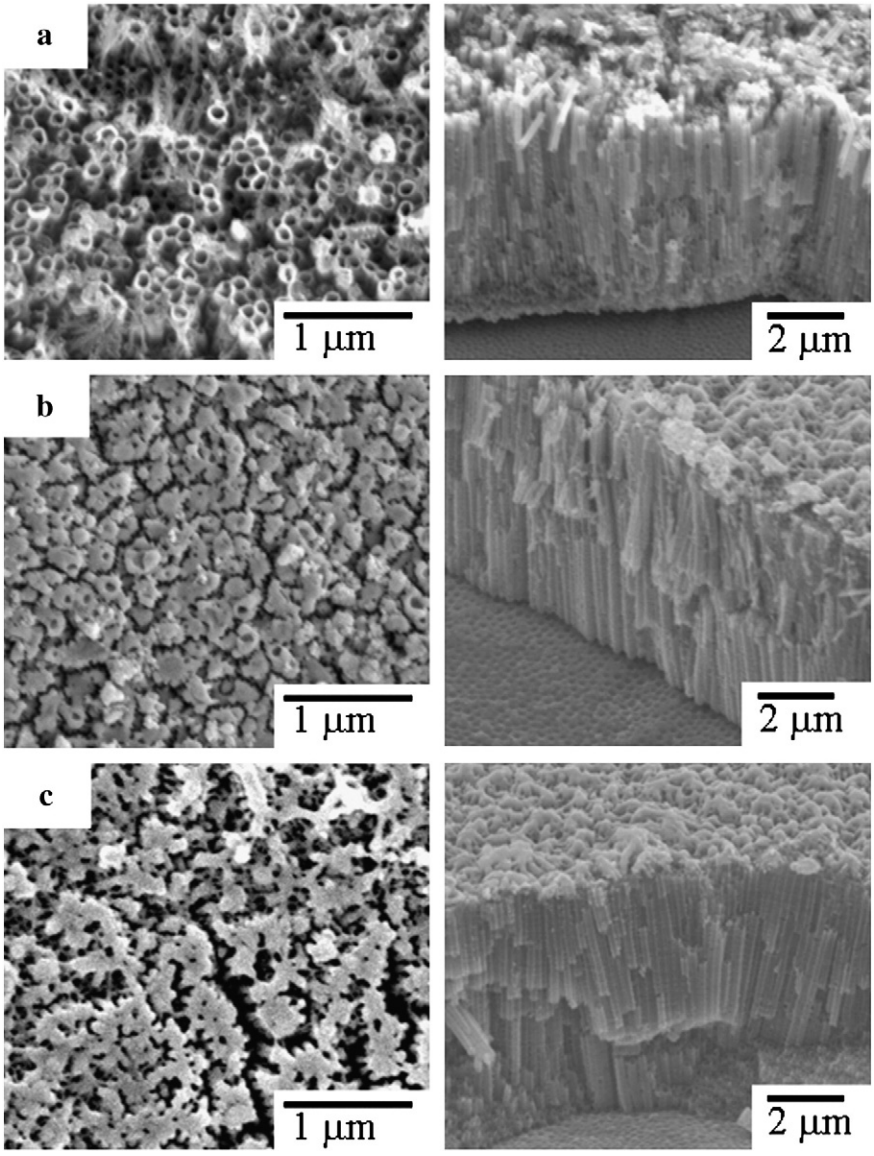

Fig. 4. Surface and cross-section morphology of the TNAs annealing by excimer laser with various fluences: (a) 67 mJc/m^2, (b) 125 mJ/cm^2, (c) 133 mJ/cm^2, (d) 267 mJ/cm^2, and (e) 400 mJ/cm^2 at 9000 shots.

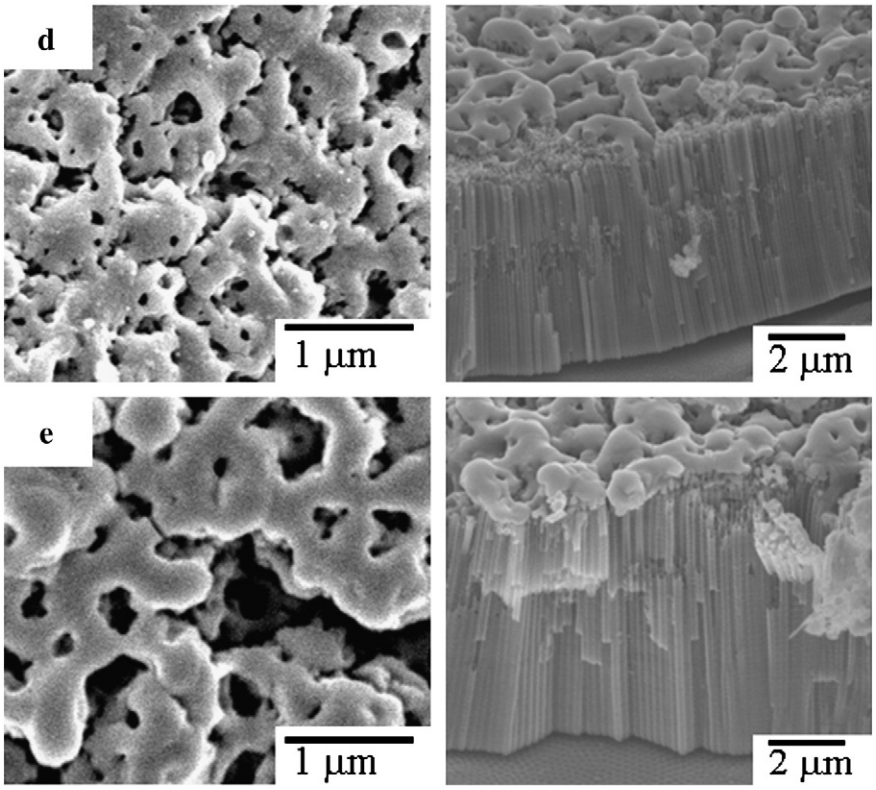

Fig. 4 (*continued*).

with increasing laser fluence [25], and the melting temperature of TiO_2 was reached as the laser fluence surpassed 125 mJ/cm^2. When the laser fluence was increased to ≥125 mJ/cm^2, the laser induced melting and coalescence near the surface, resulting in a flower-like, re-solidified layer. With increasing fluence, the re-solidified zone became larger.

On the other hand, the cross-sectional SEM images in Fig. 4a to e show that the thicknesses of TNAs do not obviously change as a function of fluence. As a result, the laser damage is limited to the area near the surface with a flower-like, re-solidified layer when higher laser fluence (≥125 mJ/cm^2) is used. This damage near the surface could be attributed to the extremely short pulse duration of the excimer laser, which has a diffusion length of the thermal wave L_T as described by Eq. (1):

$$L_T = \sqrt{D_{th}\tau} \tag{1}$$

where D_{th} is the thermal diffusivity and τ is the pulse duration. For the short pulse duration of the excimer laser, 25 ns and thermal diffusivity,

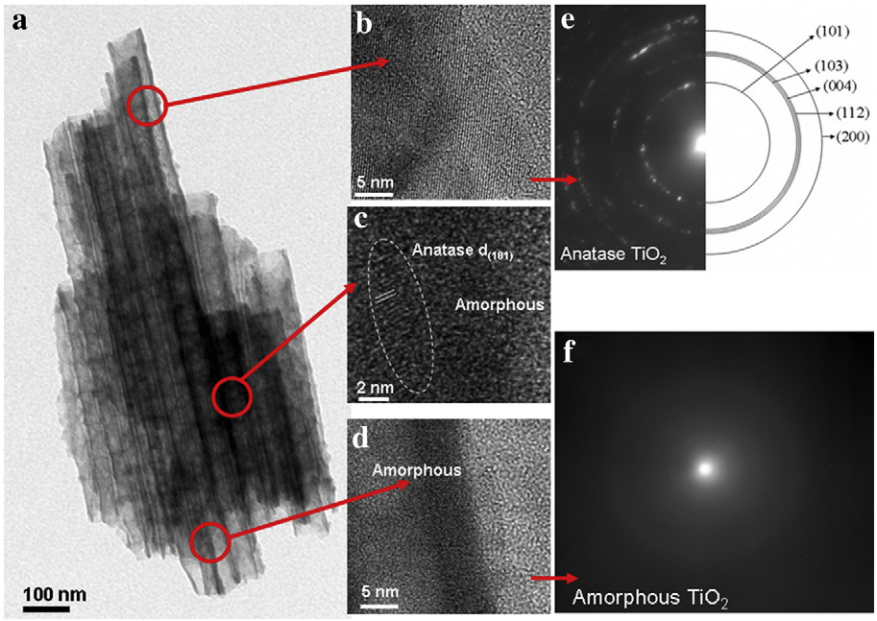

Fig. 5. TEM images of TNAs annealing by excimer laser at 400 mJ/cm^2 for 9000 shots: (a) full cross-section, (b) the top part, (c) middle part and (d) the bottom part of the cross-section, and SAD patterns of (e) the top part and (f) the bottom part of the cross-section.

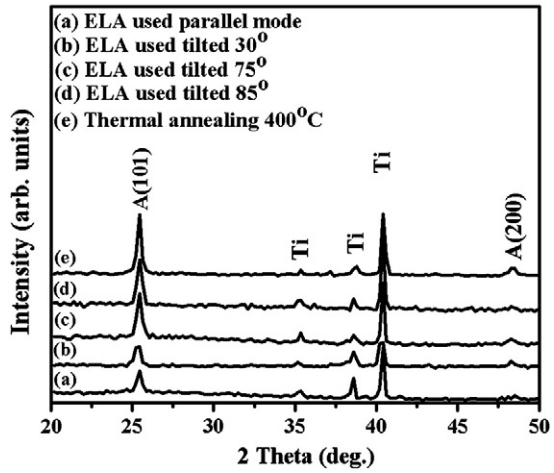

Fig. 6. The XRD patterns of TNAs annealed by conventional furnace at 400 °C for 1 h and excimer laser in parallel mode and tilted mode at a fluence of 125 mJ/cm^2 for a total of 9000 shots.

D_{th} of 0.3–0.5 cm^2/s for nanostructure [26], the thermal diffusion length, L_T, was estimated to be ~1 μm. This explains why the laser interaction and damage was localized at the irradiated surface such that only a very thin melted and re-solidified layer was formed near the surface.

To clarify the mechanism of phase transition in TNAs by laser annealing, the microstructures of TNAs along the tubes treated at 400 mJ/cm^2 fluence with 9000 shots were examined by TEM and SAD patterns. The TEM images and SAD patterns of one short TNA segment (~1.2 μm in length) are shown in Fig. 5a–f. A full cross-section TEM image of TiO_2 nanotubes (Fig. 5a) shows that the TiO_2 nanotubes had a tube diameter of 50 nm with a tube wall thickness of 15 nm. Furthermore, the microstructure of TNAs was examined by HRTEM as shown in Fig. 5b through d. To be more specific, the top part of the nanotube segment (Fig. 5b) showed crystal lattice fringes with spacings of 3.52, 2.43, 2.37, 2.33 and 1.69 Å. Their corresponding SAD patterns (Fig. 5e) include a series of continuous Debye–Scherer rings, which are identified to the spacings of $d_{(101)}$, $d_{(103)}$, $d_{(004)}$, $d_{(112)}$, and $d_{(200)}$ of anatase TiO_2, respectively [27]. The HRTEM image for the middle part of the nanotube segment (Fig. 5c) showed that anatase crystalline structure was surrounded by amorphous structure. The HRTEM image (Fig. 5d) and the corresponding featureless SAD pattern (Fig. 5f) for the bottom part of the nanotube segment clearly shows that this section was in fully amorphous phase. From SEM images and the TEM results of the microstructures along the nanotube, it is found that the phase transformation starts from the surface, and then extends downward to the middle part of the nanotube.

As a result, the temperature profile along the TiO_2 nanotubes during excimer laser pulse can be described by the one-dimensional heat conduction equation [28,29] in Eq. (2):

$$\frac{\partial T}{\partial t} = \frac{\alpha}{\rho Cp} I(z,t) + \frac{1}{\rho Cp}\frac{\partial}{\partial z}\left(k\frac{\partial T}{\partial z}\right) \tag{2}$$

where $I(z,t) = I_o(t)(1-R)e^{-\alpha z}$ is the laser pulse intensity at depth z and time t. T, α, ρ, Cp, k and R are the temperature, the absorption coefficient at 248 nm, the density, the specific heat, the thermal conductivity and the reflectivity, respectively. From Eq. (2), the temperature profile is as a function of depth. In this study, the ordered nanotube arrays are expected to exhibit a strong anisotropic thermal transport behavior due to its high porosity structure. Strong anisotropic thermal conductivity has been reported for TiO_2 nanotube arrays [30]. The thermal conductivities in the tube-length direction and in the cross-tube direction are 0.617 and 0.077–0.102 W K^{-1} m^{-1} for amorphous TNAs, 1.12 and 0.24 W K^{-1} m^{-1} for anatase TNAs, respectively [30]. However, this thermal transport from top surface to the bottom still limited the crystallinity of TNAs. Hence, in order to improve the crystallinity, a tilted mode design was carried out to

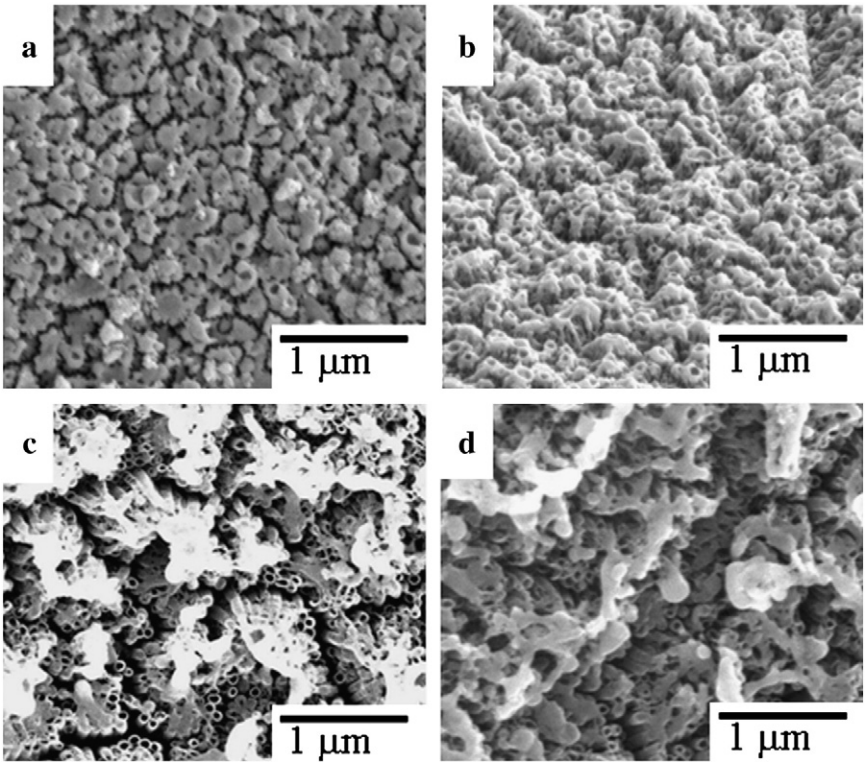

Fig. 7. Surface morphologies of TNAs for laser annealing in (a) parallel mode, (b) 30° (c) 75°, and (d) 85° in tilted mode at a fluence of 125 mJ/cm^2 for a total of 9000 shots.

analyze its effect on the structure and morphology of TNAs in the following section.

3.2. ELA treatment of TNAs in a tilted mode

In order to improve the crystallinity in TNAs obtained by parallel mode, which is limited by the penetration depth of the laser, a tilted mode of irradiation onto TNAs at various angles from 30° to 85°, as illustrated in Fig. 2b, was carried out for comparative study. Fig. 6 shows the XRD patterns of the TNAs laser-annealed in parallel mode and tilted mode at a fluence of 125 mJ/cm^2 and 9000 total shots, in addition to TNAs annealed at 400 °C for 1 h under a conventional furnace anneal. For TiO_2 treated by ELA in a tilted mode of 30°, the intensities of anatase peaks A(101) and A(200) were higher compared to those of the parallel mode, but were still lower than those obtained by conventional furnace annealing. When the tilted angle was further increased to 85°, the intensity of the A(101) peak increased with increasing tilted angle and approached that obtained by furnace annealing. This indicated that the crystallinity of TNAs was significantly enhanced in the tilted mode.

Fig. 7 illustrates the surface morphology of TNAs treated by ELA in (a) parallel mode and tilted mode: (b) 30°, (c) 75° and (d) 85° using a fluence of 125 mJ/cm^2 and 9000 total shots. For TNAs treated by ELA in parallel mode (Fig. 7a), a re-solidified layer was formed on the top of the nanotube arrays, as discussed in the previous section. In the parallel mode, 9000 shots laser pulses irradiated perpendicularly to the surface of the TNAs such that the top surface of the tubes accumulated a large amount of energy in a short duration, resulting in damage and melting. When TNAs were irradiated by the laser in tilted mode at tilted angles of 30°, 75° and 85° (Fig. 7b to d), the surface morphology of the TNAs was slightly affected by laser annealing. The damage on the surface was greatly reduced with increasing tilted angle. At a tilted angle of 85° (Fig. 7d), few tubes were broken and only a few scattered melted spots were formed on the surfaces of tubes. On the other hand, in the tilted mode, the middle part of the TNAs was irradiated by most of the laser beam. Hence, the surface morphology of TNAs was only slightly affected.

Finally, Fig. 8a–f shows the TEM images and SAD patterns of TNAs annealed by the excimer laser with a tilted angle of 85° at a fluence of 125 mJ/cm^2 for a total of 9000 shots. A full cross-section TEM image of the TiO_2 nanotubes (Fig. 8a) showed that the morphology of TiO_2 still had a highly ordered nanotube structure of about 1.2 μm in length. On the other hand, the microstructure of TNAs was examined by HRTEM images and SAD patterns, as shown in Fig. 8b through f. Small TiO_2 crystallites with a diameter of approximately ~15 nm were present in the tube walls. Furthermore, these crystallites were identified to be anatase TiO_2 by high resolution lattice image. Also, the electron diffraction patterns (Fig. 8e and f) have several continuous rings, corresponding to the spacings of $d_{(101)}$, $d_{(103)}$, $d_{(004)}$, $d_{(112)}$, and $d_{(200)}$ of anatase phase, respectively [27]. Compared to the microstructure of TNAs treated by ELA in parallel mode, ELA in tilted mode indeed significantly enhances the crystallinity of TNAs along the tube length direction.

Table 1
The XRD peak intensity ratios of TNAs annealed in conventional furnace anneal at 400 °C, 1 h and excimer laser in parallel and tilted modes at a fluence of 125 mJ/cm^2 for a total of 9000 shots.

Annealing condition	Peak intensity ratio	
	$I_{A(101)}/I_{T(101)}$	Normalized to furnace anneal
Furnace anneal 400 °C, 1 h	0.907	100%
ELA, tilted mode, 85°	0.823	91%
ELA, tilted mode, 75°	0.804	88%
ELA, tilted mode, 30°	0.589	65%
ELA, parallel mode	0.471	50%

Table 1 summarizes the XRD peak intensity ratio (I_A/I_{Ti}) of anatase (101) to Ti (101) for TNAs annealed in a conventional furnace anneal and ELA in parallel and tilted modes. For excimer laser annealing in parallel mode, the intensity of anatase (101) was 50% relative to the crystallinity of TNAs annealed by furnace annealing at 400 °C for 1 h. However, when tilted angle of 30° in tilted mode was used, the intensity of the anatase phase was increased to 65% relative to that of furnace annealing. When the angle was further increased to 85°, the intensity of the anatase phase was close to 90% in comparison to furnace annealing. This means that ELA annealing of TNAs in the tilted mode can achieve crystallinity close to that of furnace annealing with reduced treatment time (15 min).

Also, the percentage of anatase phase in the TNAs treated by ELA in tilted mode was higher than that in parallel mode. This contrasting

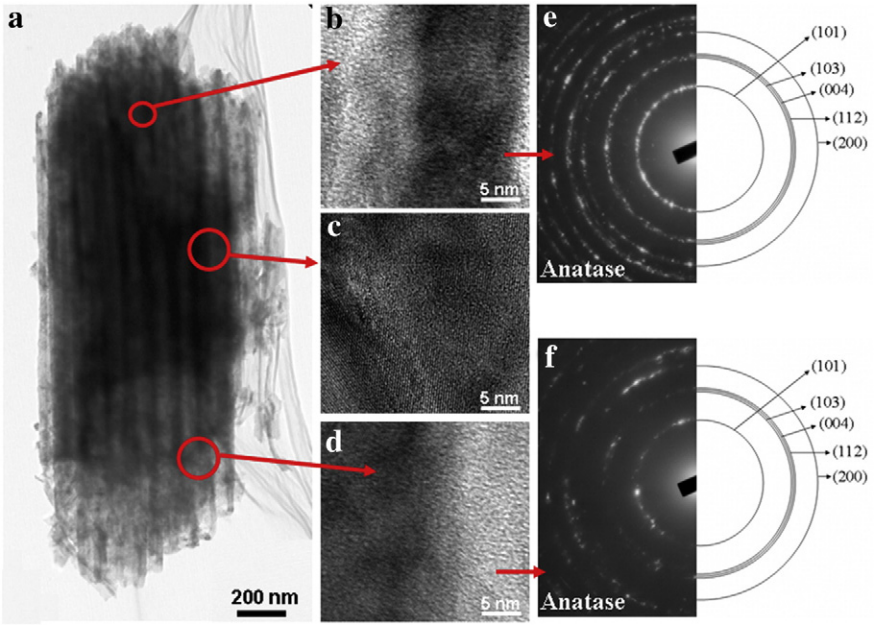

Fig. 8. TEM images of TNAs annealing by excimer laser in 85° tilted mode at a fluence of 125 mJ/cm^2 for a total of 9000 shots: (a) full cross-section, (b) the top part, (c) middle part and (d) the bottom part of the cross-section, and SAD patterns of (e) the top part and (f) the bottom part of the cross-section.

result might be explained as follows. When TNAs were treated by the laser in parallel mode, the energy of the laser beam was transferred from the top to bottom of the TNAs. Therefore, the top of the tubes was transformed from amorphous to anatase or rutile, but the middle or bottom part of the tube underwent limited phase transformation because the laser energy could not reach such a depth, due to limited thermal conduction. However, in the tilted mode, the laser beam irradiated onto the middle part of the TNAs such that the heat could be conducted toward both the top and the bottom parts of the tubes. Furthermore, in the tilted mode, the area of the laser interaction energy zone increased with increasing tilted angle, α, according to the relation $L(\alpha) = L_o(\cos\alpha)^{-1}$ [31], where L_0 is the penetration depth in the parallel mode. When a tilted angle of 85° in tilted mode was used, the penetration depth was increased to about ten times relative to that of parallel mode. Therefore, the increased area of the laser interaction energy zone in the tilted mode accounts for its better effectiveness in energy transfer, heat conduction, and phase transformation into anatase.

4. Conclusions

In this study, TiO_2 nanotube arrays (TNAs) with high aspect ratio (140:1) on Ti foil have been prepared by anodization method using NH_4F electrolyte. The structural and morphological transformations of TNAs treated by excimer laser annealing were investigated as a function of the laser fluence using parallel and tilted modes. In parallel mode, the morphology of TNAs showed the formation of the flower-like and re-solidified layer at a high fluence because the laser induced surface melting and coalescence. Also, the crystallinity of ELA-treated TNAs reached only about 50% relative to that of TNAs treated by furnace annealing at 400 °C for 1 h. This can be attributed to short penetration depth and limited one-dimensional heat transport from the surface to the bottom under extremely short pulse duration (25 ns) of the excimer laser. When a tilted mode was used, the crystallinity of TNAs treated by ELA at 85° was increased to 90% relative to that by the furnace anneal. This can be attributed to the increased area of the laser energy interaction zone and better heat conduction to both ends of the TNAs.

Acknowledgments

The authors appreciate the financial support in part by DuPont Taiwan Ltd. and National Science Council of ROC under contract number, NSC 100-3113-E-007-002.

References

[1] A. Ghicov, H. Tsuchiya, R. Hahn, J.M. Macak, A.G. Mu˜noz, P. Schmuki, Electrochem. Commun. 8 (2006) 528.
[2] R. Hahn, A. Ghicov, H. Tsuchiya, J.M. Macak, A.G. Mu˜noz, P. Schmuki, Phys. Status Solidi A 204 (2007) 1281.
[3] J.M. Macak, M. Zlamal, J. Krysa, P. Schmuki, Small 3 (2007) 300.
[4] M. Paulose, O.K. Varghese, G.K. Mor, C.A. Grimes, K.G. Ong, Nanotechnology 17 (2006) 398.
[5] K. Zhu, N.R. Neale, A. Miedaner, A.J. Frank, Nano Lett. 7 (2007) 69.
[6] T. Stergiopoulos, A. Ghicov, V. Likodimos, D.S. Tsoukleris, J. Kunze, P. Schmuki, P. Falaras, Nanotechnology 19 (2008) 235602.
[7] J.R. Jennings, A. Ghicov, L.M. Peter, P. Schmuki, A.B. Walker, J. Am. Chem. Soc. 130 (2008) 13364.
[8] M.R. Hoffmann, S.T. Martin, W. Choi, D.W. Bahnemann, Chem. Rev. 95 (1995) 69.
[9] S. Lee, C. Jeon, Y. Park, Chem. Mater. 16 (2004) 4292.
[10] M. Miyauchi, H. Tokudome, Y. Toda, T. Kamiya, H. Hosono, Appl. Phys. Lett. 89 (2006) 043114.
[11] V. Zwilling, E. Darque-Ceretti, A. Boutry-Forveille, D. David, M.Y. Perrin, M. Aucouturier, Surf. Inter. Anal. 27 (1999) 629.
[12] G.K. Mor, O.K. Varghese, M. Paulose, K. Shankar, C.A. Grimes, Sol. Energy Mater. Sol. Cells 90 (2006) 2011.
[13] L. Gao, Q. Zhang, Scr. Mater. 44 (2001) 1195.
[14] J. Ovenstone, J. Mater. Sci. 36 (2001) 1325.
[15] J.G. Yu, H.G. Yu, B. Cheng, X.J. Zhao, J.C. Yu, W.K. Ho, J. Phys. Chem. B 107 (2003) 13871.
[16] H. Kominami, J.I. Kato, S.Y. Murakami, Y. Ishii, M. Kohno, K.I. Yabutani, T. Yamamoto, Y. Kera, M. Inoue, T. Inui, B. Ohtani, Catal. Today 84 (2003) 181.
[17] Y.F. Joya, Z. Liu, Scr. Mater. 60 (2009) 467.
[18] Q. Fang, J.Y. Zhang, Z.M. Wang, J.X. Wu, B.J. O'Sullivan, P.K. Hurley, T.L. Leedham, H. Davies, M.A. Audier, C. Jimenez, J.P. Senateur, I.W. Boyd, Thin Solid Films 428 (2003) 248.
[19] C. Gopalakrishnan, K.R. Ganesh, S. Ramaswamy, K. Jeganathan, Mater. Lett. 65 (2011) 1941.
[20] H. Pan, S.H. Ko, N. Misra, C.P. Grigoropoulos, Appl. Phys. Lett. 94 (2009) 071117.
[21] P. Mitrev, G. Benvenuti, P. Hofman, A. Smirnov, N. Kaliteevskaya, Tech. Phys. Lett. 31 (2005) 908.
[22] M.Y. Hsu, W.C. Yang, H. Teng, J. Leu, J. Electrochem. Soc. 158 (2011) K81.
[23] O.V. Overschelde, S. Dinu, G. Guisbiers, F. Monteverde, C. Nouvellon, M. Wautelet, Appl. Surf. Sci. 252 (2006) 4722.
[24] S. Kitazawa, Y. Choi, S. Yamamoto, T. Yamaki, Thin Solid Films 515 (2006) 1901.
[25] O.V. Overschelde, J.M. Boisdequin, Ph. Leclère, M. Wautelet, Phys. Status Solidi C 10 (2008) 3255.
[26] J. Kim, J. Kim, M. Lee, Nanotechnology 21 (2010) 345203.
[27] V. Stengl, S. Bakardjieva, J. Subrt, L. Szatmary, Microporous Mesoporous Mater. 91 (2006) 1.
[28] S.J. Rhee, S. Kim, C.W. Sterner, J.O. White, S.G. Bishop, J. Appl. Phys. 90 (2001) 2760.
[29] M.W. Ha, S.C. Lee, J.H. Park, K.S. Seo, M.K. Han, Phys. Scr. T126 (2006) 27.
[30] L. Guo, J. Wang, Z. Lin, S. Gacek, X. Wang, J. Appl. Phys. 106 (2009) 123526.
[31] G. Foti, E. Rimini, S.U. Campisano, Phys. Status Solidi A 47 (1978) 533.